[4]Breakwell, J. V., Speyer, J. L., and Bryson, A. E., Jr., "Optimization and Control of Nonlinear Systems Using the Second Variation," *SIAM Journal of Control*, Series A, Vol. 1, No. 2, 1963, pp. 193–217.

[5]Goh, C. J., Edwards, N. J., and Zomaya, A. Y., "Feedback Control of Minimum-time Optimal Control Problems Using Neural Networks," *Optimal Control Applications and Methods*, Vol. 14, March 1993, pp. 1–16.

[6]Barnard, E., and Cole, R., "A Neural Network Training Program Based On Conjugate Gradient Optimization," Oregon Graduate Centre TR No. CSE 89-014, OR, 1989.

[7]Winfield, D. H., and Bryson, A. E., "Nonlinear Feedback Solution for Minimum-time Injection Into Circular Orbit With Constant Thrust Acceleration Magnitude," NASA CR 81474, July 1966.

Tracking Mobile Vehicles Using a Non-Markovian Maneuver Model

D. D. Sworder*
University of California, San Diego, La Jolla, California 92093
R. Vojak†
INRIA-Rocquencourt, 78153 Le Chesnay Cedex, France

Introduction

MEASUREMENTS of the motion paths of agile targets show motion at roughly constant speed for extended intervals. An osculating path is created by turning at different rates and at different times. A tractable model of such (planar) motion is given by the forth-order stochastic differential equation

$$\mathrm{d}\begin{pmatrix} X \\ Y \\ V_x \\ V_y \end{pmatrix} = \begin{bmatrix} 0 & 0 & 1 & 0 \\ 0 & 0 & 0 & 1 \\ 0 & 0 & 0 & -\omega_\psi \\ 0 & 0 & \omega_\psi & 0 \end{bmatrix} \begin{pmatrix} X \\ Y \\ V_x \\ V_y \end{pmatrix} \mathrm{d}t + \begin{bmatrix} 0 & 0 \\ 0 & 0 \\ 1 & 0 \\ 0 & 1 \end{bmatrix} \mathrm{d}\begin{pmatrix} w_x \\ w_y \end{pmatrix} \quad (1)$$

where $\{X, Y\}$ are position coordinates, and $\{V_x, V_y\}$ are associated velocities. The target is subject to two types of acceleration: a wide band omnidirectional acceleration represented by a Brownian motion $\{w_x, w_y\}$ with intensity W ($\mathrm{d}w\,\mathrm{d}w' = W\,\mathrm{d}t$), and a maneuver acceleration represented by the turn rate process $\{\omega_\psi\}$. The former influences both the speed and the direction of the target, and fits well within the linear-Gauss-Markov (LGM) modeling framework. The latter is troublesome because the sample paths of the maneuver process are better described by assuming that they are piecewise constant, taking on values from a fixed set of turn rates; $\omega_\psi \in \{a_1, \ldots, a_K\}$ (see Ref. 1 and the references therein). Treating the maneuver as an additive disturbance neglects the strict coupling between the direction of the acceleration and the velocity vector.

An image-enhanced tracking problem has been explored in numerous references using a dual-path architecture (e.g., Ref. 2) in which one path maps the image processor outputs into a maneuver estimate. The other path maps range-bearing data into an estimate of target location, with the image-information used to adjust the gains and biases in the position path. In a series of studies, it has been shown that the image-enhanced algorithms promise performance superior to that attainable from a tracker using range-bearing measurements exclusively. Image algorithms studied ranged in complexity from simply adding the image-based maneuver acceleration estimate to a conventional extended Kalman filter (EKF) (Ref. 3) to adding mean acceleration and augmenting W with image-based "pseudonoise," (called $\mathrm{EKF_p}$ in Ref. 4) and, finally, to one which used several unconventional error moments to adapt the gains of a Kalman filter (called $\mathrm{EKF_A}$ in Ref. 5). The order in which the trackers are listed is indicative of both the tracking performance and the complexity of the algorithm.

Each of the referenced algorithms was derived on the basis of a Markov maneuver model. The sojourn times of a Markov process are exponentially distributed, and there is a strong likelihood of short modal lifetimes. Paths of agile targets do not have this macroscale behavior. There is little evasive purpose for maneuvers which are short with respect to the response dynamics of the vehicle; the duration of turns are unpredictable but, clearly, not exponentially distributed. A better representation of the maneuver sojourn time is provided by a γ density; a two parameter family $\gamma(t;R, \Lambda)$, in which R controls shape and Λ controls time scale: $\gamma(t;R, \Lambda) = I_{[t>0]}\Lambda[\Gamma(R)]^{-1}(\Lambda t)^{R-1}\exp(-\Lambda t)$; $R, \Lambda > 0$. The mean of a gamma distributed random variable is $\nu = R/\Lambda$, and because it has a more intuitive connotation, ν will be used instead of Λ to indicate the time scale. Figure 1 shows three γ densities with $\nu = 1$. The maneuver sojourns described by the first ($R = 1$) would generate the Markov model used in the indicated references. The second ($R = 2$) dramatically reduces the frequency of very short lifetimes, and the third curve ($R = 5$) is sharply peaked, with more quasipredictable intervals. The densities with $R > 1$ mirror more closely the turn intervals for an agile target. This paper compares non-Markovian ($R > 1$) tracking algorithms with simpler Markov ($R = 1$) versions on a coast-turn-cost path. It has been shown that the performance of $\mathrm{EKF_P}$ improves with a non-Markov maneuver model (Ref. 6). Unfortunately, the $R > 1$ algorithms are more complicated to implement, and this is particularly true for the $\mathrm{EKF_A}$ tracker. It is shown here that a simple (Markov) $\mathrm{EKF_A}$ is superior to the $\mathrm{EKF_P}$ even when the latter uses a nonMarkov acceleration model. An $\mathrm{EKF_A}$ for $R > 1$ has improved response, but not to a degree commensurate with the increase in algorithmic complexity. This relative improvement is found even when as the realized sojourn times differ from their mean values. This suggests that the simplest EKF is a suitable for applications that are not well described by a Markov model.

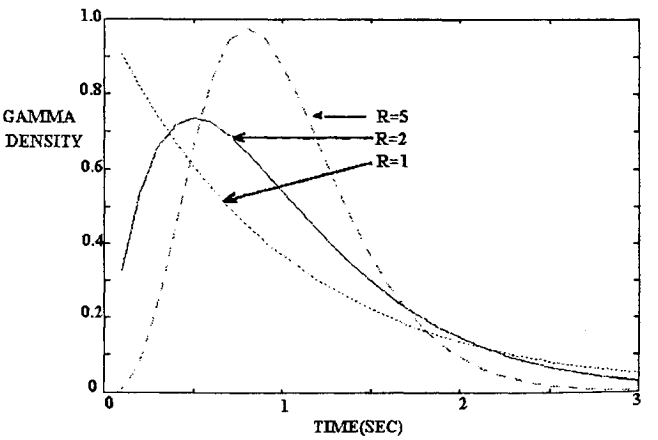

Fig. 1 Gamma densities for different values of *R*.

Received May 3, 1993; revisision received July 5, 1993; accepted for publication July 13, 1993.

*Professor, Department of Electrical and Computer Engineering.
†Research Associate.

Review of Measurement Models and Tracking Algorithms

In this application it will be assumed that range and bearing are measured from a fixed location with independent Gaussian errors. For use in an EKF, this measurement is localized; the "linearized" measurement takes the form

$$y_t = \mathrm{D}x_t + n_t \tag{2}$$

at observation times. In Eq. 2, $\{n_t\}$ is a white noise measurement noise with covariance $R_x > 0$.

The image-link maps a sequence of measurements of the angular orientation of the target with respect to the sensor-target line of sight into an estimate of maneuver status. In summary, this is done as follows. The image processor receives data frames at a rate of λ frames/s, and places each image into one of L equally spaced orientation bins. The output of the image processor can be written as an L-dimensional counting process $\{\sigma_t\}$, the ith component of which is the number of times the target has been placed in angular bin i on the interval $[0, t]$. Denote the true orientation bin at time t by the indicator vector ρ_t; $\rho_t = \boldsymbol{e}_i$ if the current target orientation is in the ith bin. (Let $\boldsymbol{e}_i$ be a unit vector with a 1 in the ith component in the appropriate space.) The quality of image interpretation is determined by the $L \times L$ discernibility matrix $\boldsymbol{p} = [\boldsymbol{p}_{ij}]$ where $\boldsymbol{p}_{ij}$ is the probability that bin i will be selected by the processor if bin j contains the true target orientation at time of image creation; $\boldsymbol{p}_{ij} = \wp(\Delta\sigma_i = 1/\rho = e_j)$. The precision of motion inference is a function of three things: the frame rate λ, the ability of the image to correctly classify a single image $\boldsymbol{p}$, and the tempo of the encounter.

The sequence of imager outputs is interpreted by a temporal processor to give the relative likelihoods of the various rate modes using a fairly simple procedure. Denote the information pattern generated by $\{\sigma_t\}$ by $\{Z_t\}$, and the conditional expectation of the various processes with respect to the appropriate observation by a caret superscript. Denote the maneuver mode by α_t, a K-dimensional unit vector indicating the current turn rate; if $\omega_\psi = a_i$, then $\alpha_t = \boldsymbol{e}_i$. The composite maneuver status of the target is given by $\{\phi_t\} = \{\alpha_t \otimes \rho_t\}$, the Kronecker product of maneuver and orientation. For a specific turn rate ($\alpha_t = \boldsymbol{e}_i$), suppose the angular bin sequence is a Markov process with generator Q^i. Then $\{\phi_t\}$ is a Markov process with $KL \times KL$-dimensional generator $Q = (q \otimes \boldsymbol{I}_L) + \mathrm{diag}(Q^i)$ where the second term is to be interpreted as block diagonal. It is shown in Ref. 7 that the Z_t conditional mean of $\{\phi_t\}$ is generated by the equation involving a process $\{\vartheta_t\}$ constant between observations and increments given by $\Delta\vartheta_t = \lambda \boldsymbol{p}' \mathrm{diag}(\hat{\lambda}^{-1})\,\Delta\sigma$. This is specifically as follows.

Between observations:

$$\left(\frac{\mathrm{d}}{\mathrm{d}}t\right)\hat{\phi}_t = Q'\hat{\phi}_t \tag{3a}$$

At an observation time:

$$\hat{\phi}^+ = \mathrm{diag}(\Delta\vartheta)\hat{\phi}^- \tag{3b}$$

The conditional probabilities of the various turn rates can be extracted from $\{\hat{\phi}_t\}$: $\hat{\alpha}_t = [\wp\{\omega_\psi = a_i | Z_t\}] = (\boldsymbol{I}_K \otimes \boldsymbol{1}_L \boldsymbol{I}_L')\hat{\phi}_t$. The gain-adaptive tracker $\mathrm{EKF_A}$ (detailed in Ref. 5) is given by the following algorithm:

Between observations:

$$\mathrm{d}\hat{x}_t = \{\Sigma_i A_i[(P_{x\phi})_{\cdot i} + \hat{x}_t\hat{\phi}_i]\}\,\mathrm{d}t \tag{4a}$$

At a location measurement:

$$\Delta\hat{x}_t = P_{xx}D'(DP_{xx}D' + R_x)^{-1}\Delta\nu_t \tag{4b}$$

At an image measurement:

$$\Delta\hat{x}_i = P_{x\phi}\Delta\vartheta_t \tag{4c}$$

where $\Delta\nu_t = y_t - D\hat{x}_t$ is the increment in the innovations process, and P_{xx} and $P_{x\phi}$ are second central moments of the estimation error. The tracker updates come as a complementary pair: location and image. The location update has a conventional form, whereas the image update involves increments in the $\{\vartheta_t\}$ process defined earlier. Note that the second moments $\{P_{xx}\}$ and $\{P_{x\phi}\}$ must be computed to implement $\mathrm{EKF_A}$, and this is not easy to do. The relevant equations are given in Ref. 5 and will not be repeated here. It is primarily in this calculation that $\mathrm{EKF_A}$ differs from the more conventional extended Kalman filters.

The simpler filter, $\mathrm{EKF_P}$, treats the acceleration as essentially additive but augments the $\{P_{xx}\}$ calculation with the conditional variance of the maneuver state.

Between observations:

$$\mathrm{d}\hat{x}_t = \hat{A}_t\hat{x}_t\,\mathrm{d}t \tag{5a}$$

At a location measurement:

$$\Delta\hat{x}_t = P_{xx}D'(DP_{xx}D' + R_x)^{-1}\Delta\nu_t \tag{5b}$$

Although similar in appearance to Eqs. (4), the second moment calculations are considerably different, with those of $\mathrm{EKF_P}$ being much more conventional than those of $\mathrm{EKF_A}$.

Use of a Non-Markovian Maneuver Model

To represent the maneuver dynamics within the framework just developed, note that if $\{\omega_\psi\}$ is a finite state renewal process, it is distinguished by two things; the sequencing of modes, e.g., $i \to j$ at time t ($\alpha_t = e_i$ and $\alpha_t = e_j$), and the duration in each maneuver mode. Both are unpredictable (random). In a renewal process, the state sequence is Markovian with transition matrix P: $P_{ij} = \wp(i \to j \text{ at } t | \alpha_{t-} = e_i \text{ and } \Delta\alpha_t \neq 0)$. The sojourn times are independent given the "past" sequence of modal transitions, and for the purposes of this study, duration of the ith maneuver mode ($i \in \boldsymbol{K}$) will be assumed to be gamma distributed with integer index R_i. Instead of the single transition rate matrix q, the maneuver dynamics are now characterized by the pair $\{P, \gamma(t; R_i, \nu_i);\ i \in \boldsymbol{K}\}$.

If R_i are all equal to 1, $\{\alpha_t\}$ is a Markov process; if any of the R_i are not 1, $\{\alpha_t\}$ is non-Markovian. The non-Markovian maneuver model can, however, be integrated into the earlier algorithms by expanding the dimension of the maneuver state space, creating set of submaneuvers. The true maneuver state space is of dimension K. Associate to the set $\{R_i: i \in \boldsymbol{K}\}$ the set of integers $\boldsymbol{A} = \boldsymbol{A}_1 \cup \ldots \cup \boldsymbol{A}_K$, where $\boldsymbol{A}_1 = \{1, \ldots, R_1\}$, $\boldsymbol{A}_2 = \{R_1 + 1, \ldots R_1 + R_2\}$ and so on; each substantive maneuver mode is decomposed into R_i pseudomodes, each of which is associated with the same turn rate. The γ-renewal process is Markov in the larger state space. To find its generator q define for every $p \in \boldsymbol{K}$ the maximum and minimum pseudomode indices, $r_p = \min_k(k \in \boldsymbol{A}_P)$, and $s_p = \max_k(k \in \boldsymbol{A}_P)$. Then r_P is the entrance state into the pth maneuver, and s_P is its exit. Note that the dimension of the γ-renewal model is s_K. To maintain both the mean sojourn times and the sequencing of modes implicit in q, q should be chosen as follows: $q_{ij} =$ [1) $R_p q_{pp}$ if $i, j \in \mathbf{A}_p$ and $j = i$; 2) $-R_p q_{pp}$ if $i, j \in \mathbf{A}_p$ and $j = i + 1$; 3) $R_p q_{pk}$ if $i = s_p$, $j = r_k$ and $p \neq k$; or, finally, 4) 0 otherwise]. With these changes $\mathrm{EKF_A}$ and $\mathrm{EKF_P}$ can be deduced by replacing the generator of the (maneuver $\times$ orientation) process by the $(s_K L \times s_K L)$ matrix $\mathfrak{Q} = (q \otimes \boldsymbol{I}_L) + \mathrm{diag}(\mathfrak{Q}^i)$ where $\mathfrak{Q}^k = Q^i$ if $k \in \boldsymbol{A}_i$. Note that the calculation of $\{\hat{\alpha}_t\}$ goes up as s_K/K, and this calculation is common to both $\mathrm{EKF_A}$ and $\mathrm{EKF_P}$. In $\mathrm{EKF_P}$ it is not necessary to compute a full set of

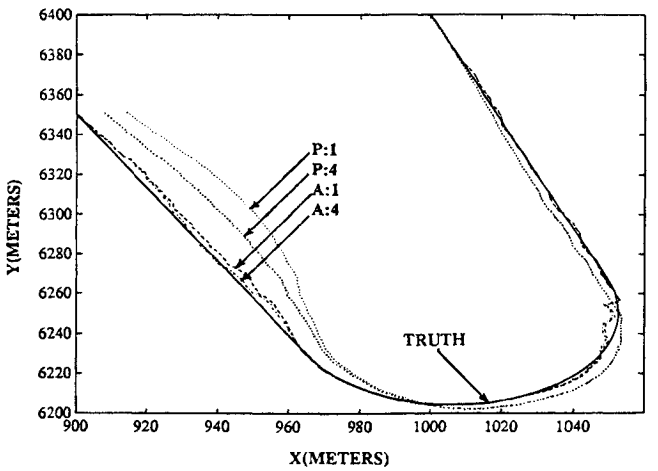

Fig. 2 Location performance; EKF_P and EKF_A for $R = 1$ and $R = 4$.

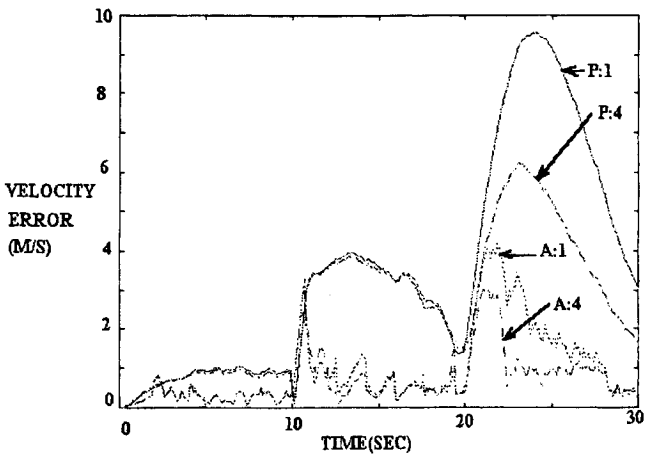

Fig. 3 Velocity errors vs time: EKF_P and EKF_A for $R = 1$ and $R = 4$.

moments, but the number of the second moment matrices in EKF_A increases rapidly with s_k/K.

Performance Comparison of the Extended Kalman Filters

Consider a coast-turn-coast path studied in the references. The target is initially located at $(X_0, Y_0) = (1.0, 6.4)$ km, and moving at constant velocity $(V_{x0}, V_{y0}) = (5.0, -13.3)$ m/s for $t \in [0, 10)$ s. A 0.3 rad/s turn is made during $t \in [10, 20)$, after which the target returns to constant velocity motion. Figure 2 shows the target path (labeled truth) without the wideband acceleration. Tracking will be accomplished with range-bearing and image measurements taken at a 10/s rate from sensors located at (0, 0). Location errors have standard deviation 5.0 m and 0.25 deg, respectively. The imager places the target in angular bins of width 30 deg. A taxonomy used in Ref. 5 considers errors of three types: uniformly distributed errors across the angular bin set; nearest neighbor errors in which the target is placed in a neighboring angular bin; and projection error in which the target is placed symmetrically with respect a perpendicular to the line-of-sight. Specifically, suppose the error triple is (0.01, 0.03, 0.29); the imager misclassifies its observation one-third of the time.

The tempo of the encounter is determined by the acceleration dynamics. The omnidirectional accelerations will be assumed to be slight: $W = 0.01I\ (\mathrm{m/s^2})^2$. The maneuver state space will be three dimensional; $\{a_1 = \text{coast}, a_{2,3} = \pm 0.3\ \mathrm{rad/s}\}$, with the chain $\{\alpha_t\}$ symmetric about the coasting mode. The elements of the q matrix are determined jointly by the mean sojourn times in each acceleration mode; $[\nu_i, i = 1, 2, 3; \nu_2 = \nu_3\}$, and the transition probabilities from a maneuver to the nonmaneuvering mode. Let $q_1 = \wp(\alpha_t = e_1 | \alpha_t = e_2 \text{ and } \Delta\alpha_t \neq 0)$. Then q_1 measures the fraction of times that a maneuver ends in a coasting motion; e.g., $q_1 = 0$ implies pure jinking motion, and $q_1 = 1$ always interjects coasting between turns. Specifically, consider an encounter with the following tempo: $\nu_1 = 20$ s, $\nu_2 = 10$ s, $q_1 = 1.0$.

The renewal lifetime model selected will be given by the γ-renewal functions for $R = 4$. Figure 2 shows the response of four trackers to the (α_t); $1 \rightarrow 3 \rightarrow 1$ scenario: EKF_P and EKF_A for $R = 1$ and $R = 4$ [labeled P (alternately A): 1 (alternately 4)]. To display biases, 20-trial mean sample paths are shown rather than the (noisier) single sample paths. All of the filters perform well in the premaneuver phase but deviate both during and after a turn. Figure 3 shows corresponding velocity profiles, and the EKF_P curves are not good. As in position, EKF_A ($R = 4$) is superior to its fellows in peak performance. It is better than EKF_P during the turn and much quicker to reduce transient errors to manageable levels. Performance improvement of EKF_A is, however, not commensurate with complexity; i.e., R. Though not shown, the relative response of $\{\alpha_t\}$ for longer or shorter sojourns is easily found. For off-nominal conditions, EKF_A is surprisingly robust. Although not shown here, the $\{P_{xx}\}$ process computed for EKF_A ($R = 4$) differs little from that shown in Fig. 8 of Ref. 5. The explanation for the improvement in EKF_A with R derives more from the mixed moment $P_{x\phi}$.

Conclusions

This paper studies the performance improvement attainable from an image enhanced tracking filter as the maneuver model is made more accurate. In contrast with simpler implementations, the gain adaptive extended Kalman filter (EKF_A) does well even when a Markov model is used. This filter appears to be sufficiently robust as to not need the additional computation that a high accuracy maneuver model entails. This is fortunate, because the computational load of the algorithm goes up rapidly as the maneuver sojourns differ from exponential.

Acknowledgments

This research was partially supported by a grant from the Hughes Aircraft Co., El Sequndo CA, and by the MICRO Program of the State of California under Project 92-155.

References

[1] Cloutier, J. R., Evers, J. H., and Feeler, J. J., "Assessment of Air-to-Air Missile Guidance and Control Technology," *IEEE Control Systems*, Oct. 1989, pp. 27–34.

[2] Kendrick, J. D., Maybeck, P. S., and Reid, J. G., "Estimation of Aircraft Target Motion Using Orientation Measurements," *IEEE Transaction on Aerospace and Electronic Systems*, Vol. AES-17, March 1981, pp. 254–259.

[3] Hutchins, R. G., and Sworder, D. D., "Image Fusion Algorithms for Tracking Maneuvering Targets," *Journal of Guidance, Control, and Dynamics*, Vol. 15, No. 1, 1992, pp. 175–184.

[4] Sworder, D. D., and Hutchins, R. G., "Improved Tracking of an Agile Target," *Journal of Guidance, Control, and Dynamics*, Vol. 15, No. 5, 1992, pp. 1281–1284.

[5] Sworder, D. D., Vojak, R., and Hutchins, R. G., "Gain Adaptive Tracking," *Journal of Guidance, Control, and Dynamics*, Vol. 16, No. 5, 1993, pp. 865–873.

[6] Sworder, D. D., Vojak, R., Hutchins, R. G., and Kent, M., "Renewal Models for Maneuvering Targets," *IEEE Transactions on Aerospace and Electronic Systems*, April 1994.

[7] Sworder, D. D., and Hutchins, R. G., "Maneuver Estimation Using Measurements of Orientation," *IEEE Transactions on Aerospace and Electronic Systems*, Vol. AES-26, No. 5, 1990, pp. 625–638.